Article

Chimera Diimine Ligands in Emissive [Cu(P^P)(N^N)][PF$_6$] Complexes

Marco Meyer [ID]**, Fabian Brunner** [ID]**, Alessandro Prescimone** [ID]**, Edwin C. Constable** [ID] **and Catherine E. Housecroft *** [ID]

Department of Chemistry, University of Basel, BPR 1096, Mattenstrasse 24a, CH-4058 Basel, Switzerland; marco.meyer@unibas.ch (M.M.); fabian.brunner@unibas.ch (F.B.); alessandro.prescimone@unibas.ch (A.P.); edwin.constable@unibas.ch (E.C.C.)

* Correspondence: catherine.housecroft@unibas.ch; Tel.: +41-61-207-1008

check for updates

Abstract: The syntheses and characterizations of the chelating ligand 6-chloro-6′-methyl-2,2′-bipyridine (6-Cl-6′-Mebpy) and of the copper(I) compounds [Cu(POP)(6-Cl-6′-Mebpy)][PF$_6$] and [Cu(xantphos) (6-Cl-6′-Mebpy)][PF$_6$] (POP = bis(2-(diphenylphosphanyl)phenyl)ether and xantphos = 4,5-bis (diphenylphosphanyl)-9,9-dimethyl-9*H*-xanthene) are described. The single crystal structures of both complexes were determined; the copper(I) ion is in a distorted tetrahedral environment and in [Cu(xantphos)(6-Cl-6′-Mebpy)][PF$_6$], the disorder of the 6-Cl-6′-Mebpy ligand indicates there is no preference of the 'bowl'-like cavity of the xanthene unit to host either the methyl or chloro-substituent, consistent with comparable steric effects of the two groups. The electrochemical and photophysical properties of [Cu(POP)(6-Cl-6′-Mebpy)][PF$_6$] and [Cu(xantphos)(6-Cl-6′-Mebpy)][PF$_6$] were investigated and are compared with those of the related compounds containing 6,6′-dichloro-2,2′-bipyridine or 6,6′-dimethyl-2,2′-bipyridine ligands. Trends in properties of the [Cu(P^P)(N^N)]$^+$ complexes were consistent with 6-Cl-6′-Mebpy behaving as a combination of the two parent ligands.

1. Introduction

Light-emitting diode (LED) and organic LED (OLED) solid-state lighting technologies are firmly embedded in our society [1]. Light-emitting electrochemical cells (LECs) represent a less well developed, but nonetheless promising, area of solid-state lighting [2,3]. Among the compounds targeted for emissive components in the active layers of LECs are heteroleptic [Cu(P^P)(N^N)]$^+$ complexes in which P^P is a wide bite-angle bisphosphane [4] and N^N contains a diimine metal-binding domain. Investigations in this field were inspired by the work of McMillin and coworkers who showed that [Cu(P^P)(N^N)]$^+$ complexes possess low-lying metal-to-ligand charge transfer (MLCT) excited states [5,6]. In the last decade, it has been shown that [Cu(P^P)(N^N)]$^+$ complexes exhibit thermally activated delayed fluorescence (TADF) [7,8]. This phenomenon involves fast intersystem crossing from the lowest-lying singlet excited state (S$_1$) to the triplet excited state (T$_1$); because the latter is long-lived and shows a relatively slow phosphorescence, thermal repopulation of the singlet excited state via a reverse intersystem crossing occurs with a concomitant fluorescence emission from S$_1$. This process significantly increases the photoluminescent quantum yield (PLQY), making [Cu(P^P)(N^N)]$^+$ complexes of particular interest for use in LECs and allows the harvesting of both triplet and singlet excited states which are generated in a 3:1 ratio [7,8].

The most frequently used wide bite-angle bisphosphanes in these compounds are 4,5-bis (diphenylphosphanyl)-9,9-dimethyl-9*H*-xanthene (xantphos, IUPAC PIN (9,9-dimethyl-9*H*-xanthene-4,5-diyl)bis(diphenylphosphane)) and bis(2-(diphenylphosphanyl)phenyl)ether (POP, IUPAC PIN

oxydi(2,1-phenylene)] bis(diphenylphosphane)). The structures of POP and xantphos are shown in Scheme 1. The diimine ligand is typically a derivative of 2,2′-bipyridine (bpy) or 1,10-phenanthroline (phen). Despite the wide range of N^N ligands introduced into [Cu(P^P)(N^N)]$^+$ complexes [9], simple ligands including 6-alkyl-2,2′-bipyridines, 6,6′-dialkyl-2,2′-bipyridines [10,11], 6-alkyloxy-2,2′-bipyridines [12], 6,6′-bis(alkyloxy)-2,2′-bipyridines [13], 6-thioalkyl-2,2′-bipyridines [12] and 6,6′-dihalo-2,2′-bipyridines [14] often lead to the highest PLQY values and the best electroluminescence (EL) performances in LECs.
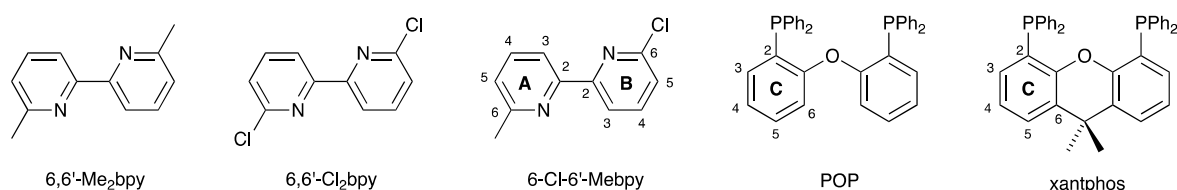
Scheme 1. The structures of the N^N ligands 6,6′-Me$_2$bpy, 6,6′-Cl$_2$bpy and 6-Cl-6′-Mebpy, and of the P^P ligands POP and xantphos. Atoms labeling is used for NMR spectroscopic assignments; the phenyl rings in the PPh$_2$ units in POP and xantphos are labeled **D**.

Powdered samples of [Cu(POP)(6,6′-Me$_2$bpy)][PF$_6$] and [Cu(xantphos)(6,6′-Me$_2$bpy)][PF$_6$] (6,6′-Me$_2$bpy = 6,6′-dimethyl-2,2′-bipyridine, Scheme 1) exhibit PLQYs of 43.2% [10] and 37% [11], respectively. The introduction of the methyl groups is critical to improving PLQY values and performance in LECs [10,11,15]. A LEC with [Cu(POP)(6,6′-Me$_2$bpy)][PF$_6$] in the active layer reached a maximum luminance of 53 cd m^{-2} and maximum efficacy of 5.2 cd A^{-1} [10], values which are appreciably higher than for [Cu(POP)(bpy)][PF$_6$] (1.64 cd A^{-1}) [15]. However, the LEC turn-on times were in the order of minutes [10,11]. Changing the methyl substituents for chlorine substituents (Scheme 1) results in a decrease in PLQY values with powdered [Cu(POP)(6,6′-Cl$_2$bpy)][PF$_6$] and [Cu(xantphos)(6,6′-Cl$_2$bpy)][PF$_6$] exhibiting PLQYs of 15% and 17%, respectively. The performances of LECs with [Cu(POP)(6,6′-Cl$_2$bpy)][PF$_6$] and [Cu(xantphos)(6,6′-Cl$_2$bpy)][PF$_6$] in the active layers were promising with rapid LEC turn-on times of <5 s and 12 s, respectively, and maximum luminances of 121 and 259 cd m^{-2}, respectively, when the average current density was 100 A m^{-2} [14]. These results suggested the idea of a diimine ligand that incorporated both chlorine and methyl substituents. Here, we report the synthesis and spectroscopic and structural properties of the copper(I) complexes [Cu(POP)(6-Cl-6′-Mebpy)][PF$_6$] and [Cu(xantphos)(6-Cl-6′-Mebpy)][PF$_6$]. Surprisingly, reports of the ligand 6-Cl-6′-Mebpy (Scheme 1) are confined to the patent literature [16] and to inclusion in a theoretical study of redox potentials, pK_a values of [H$_2$bpy]$^{2+}$ and solubilities of a wide range of bpy derivatives [17].

2. Results and Discussion

2.1. Synthesis and Characterization of 6-Cl-6′-Mebpy

The preparation of 6-Cl-6′-Mebpy reported in the patent literature [16] involved the Grignard reaction of MeMgBr with 6,6′-Cl$_2$bpy. We favored a Negishi coupling between 2,6-dichloropyridine and 6-methyl-2-pyridinylzinc bromide under microwave conditions, which led to 6-Cl-6′-Mebpy in a 23.5% yield after purification. The base peak in the electrospray mass spectrum was observed at *m/z* 205.02 and was assigned to the [M + H]$^+$ ion. The isotopomer distribution (Figure S1 in the supplementary materials) was as predicted. The ^{1}H and ^{13}C{^{1}H} NMR spectra were assigned using COSY, NOESY, HMQC and HMBC methods. In the ^{1}H NMR spectrum, two sets of pyridine ring signals (Figure S2) and the presence of one methyl signal were consistent with the structure of 6-Cl-6′-Mebpy shown in Scheme 1. The HMQC and HMBC spectra are displayed in Figures S3 and S4.

2.2. Synthesis and Characterization of [Cu(POP)(6-Cl-6′-Mebpy)][PF$_6$] and [Cu(xantphos)(6-Cl-6′-Mebpy)][PF$_6$]

The syntheses of the POP and xantphos-containing [Cu(PˆP)(bpy)][PF$_6$] compounds require two different strategies, for reasons we have previously discussed in detail [11,12]. Treatment of [Cu(MeCN)$_4$][PF$_6$] with POP in CH$_2$Cl$_2$ followed, after two hours, by the addition of 6-Cl-6′-Mebpy resulted in the formation of [Cu(POP)(6-Cl-6′-Mebpy)][PF$_6$]. In contrast, [Cu(xantphos)(6-Cl-6′-Mebpy)] [PF$_6$] was prepared in a one-pot process by combining [Cu(MeCN)$_4$] [PF$_6$], xantphos and 6-Cl-6′-Mebpy. After precipitation from CH$_2$Cl$_2$ solutions by the addition of Et$_2$O, the complexes were isolated in 72.0% and 87.0% yields, respectively. The electrospray mass spectra of the two compounds are shown in Figures S5 and S6. The highest mass peak corresponded to the [M − PF$_6$]$^+$ cation (*m/z* = 805.12 for [Cu(POP)(6-Cl-6′-Mebpy)]$^+$ and *m/z* = 845.16 for [Cu(xantphos)(6-Cl-6′-Mebpy)]$^+$). Loss of the 6-Cl-6′-Mebpy ligand from the complex cation led to the base peak in each mass spectrum (*m/z* = 601.09 and 641.10, respectively).

The solution NMR spectra of [Cu(POP)(6-Cl-6′-Mebpy)][PF$_6$] and [Cu(xantphos)(6-Cl-6′-Mebpy)][PF$_6$] were recorded in acetone-*d*$_6$ and a comparison of the aromatic regions of the ^{1}H NMR spectra is given in Figure 1. The atom labeling for the NMR spectroscopic assignments is given in Scheme 1. As in the ^{1}H and ^{13}C{^{1}H} NMR spectra of related compounds [11,12,18,19], two sets of signals are observed for the phenyl rings of the PPh$_2$ groups. In Figure 1, these are labeled D and D′. In the NOESY spectrum of each complex, cross-peaks between signals for the methyl group of 6-Cl-6′-Mebpy and one set of protons-D2 were observed, defining D2′ as the *ortho*-protons on the phenyl rings closest to the NˆN ligand. Combined use of NOESY and HMQC allows the ^{13}C resonances for C^{D2} and C$^{D2′}$ to be distinguished (Figure 2). The distinction between the sets of phenyl rings is more clearly recognizable in the structural discussion that follows later.
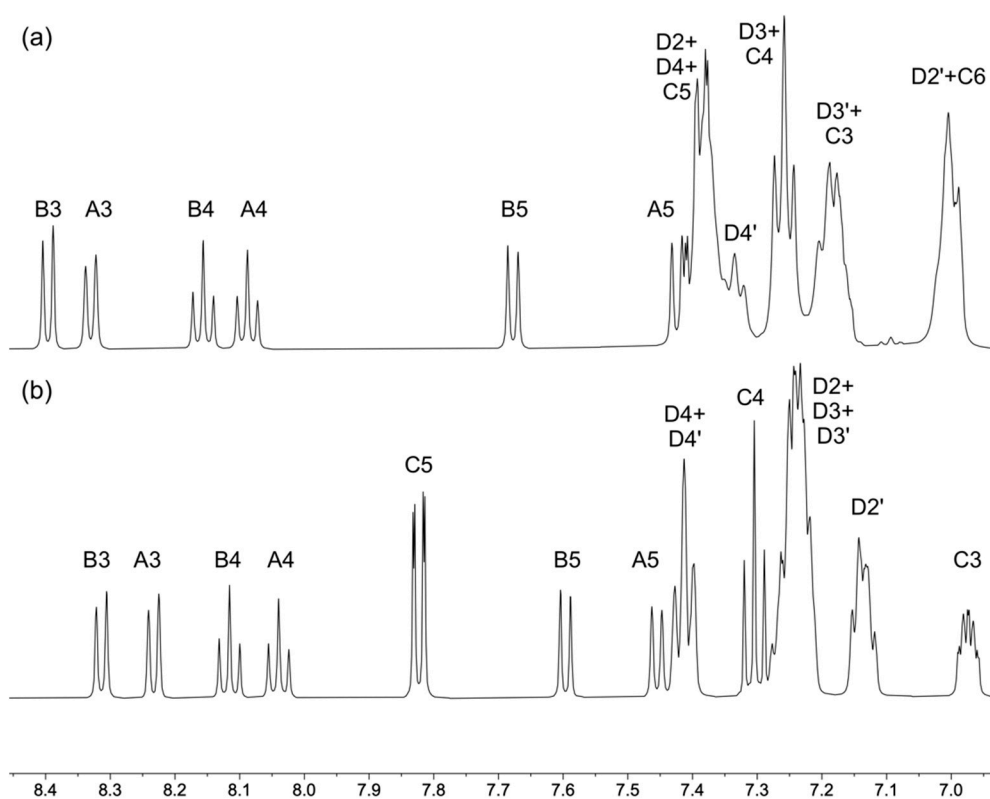

Figure 1. The aromatic regions of the ^{1}H NMR spectra of (**a**) [Cu(POP)(6-Cl-6′-Mebpy)][PF$_6$] and (**b**) [Cu(xantphos)(6-Cl-6′-Mebpy)][PF$_6$] (500 MHz, 298 K, acetone-*d*$_6$). The labeling scheme is shown in Scheme 1. Scale: δ/ppm.
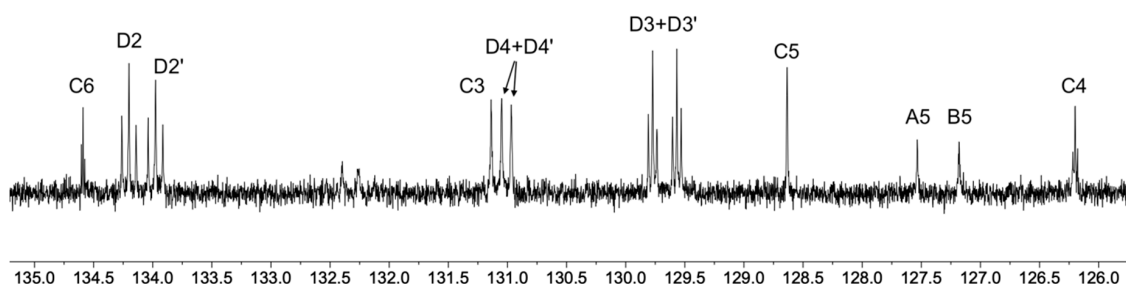
Figure 2. Part of the ^{13}C{^{1}H} NMR spectrum of [Cu(xantphos)(6-Cl-6'-Mebpy)][PF$_6$] (126 MHz, 298 K, acetone-d_6) evidencing the two environments of the PPh$_2$ phenyl rings (rings D). See Scheme 1 for atom numbering. Scale: δ/ppm.

Single crystals of [Cu(POP)(6-Cl-6'-Mebpy)][PF$_6$] were grown by diffusion of *n*-hexane into an acetone solution of the compound. For [Cu(xantphos)(6-Cl-6'-Mebpy)][PF$_6$], diffusion of Et$_2$O into a CH$_2$Cl$_2$ solution of the complex was used to grow crystals. The POP- and xantphos-containing compounds crystallize in the monoclinic *P*2$_1$/*c* and triclinic *P*–1 space groups, respectively. The copper atom in each complex cation is in the expected distorted tetrahedral geometry with two chelating ligands (Figure 3). The structure of the [Cu(POP)(6-Cl-6'-Mebpy)]$^+$ cation was severely disordered in both the N^N and POP domains. Within the POP ligand, half of the {(C$_6$H$_4$)$_2$O} unit and two phenyl rings of one PPh$_2$ group were also disordered, and each fragment was modeled with a 50% site occupancy. The Cl and Me substituents in the 6-Cl-6'-Mebpy ligand in both compounds were disordered and were modeled over two sites, each with a 50% occupancy. The disorders do not affect the {CuP$_2$N$_2$}-coordination sphere and relevant bond lengths and angles are given in Table 1. ORTEP representations of the complex cations and the disorders in the [Cu(POP)(6-Cl-6'-Mebpy)]$^+$ cation are depicted in Figures S12–S14 in the supporting information. In the [Cu(POP)(6-Cl-6'-Mebpy)]$^+$ cation, the bpy unit is twisted with an angle between the least squares planes through the two pyridine rings of 19.5°. The corresponding angle in the [Cu(xantphos)(6-Cl-6'-Mebpy)]$^+$ cation is 5.7°.

(a)   (b)
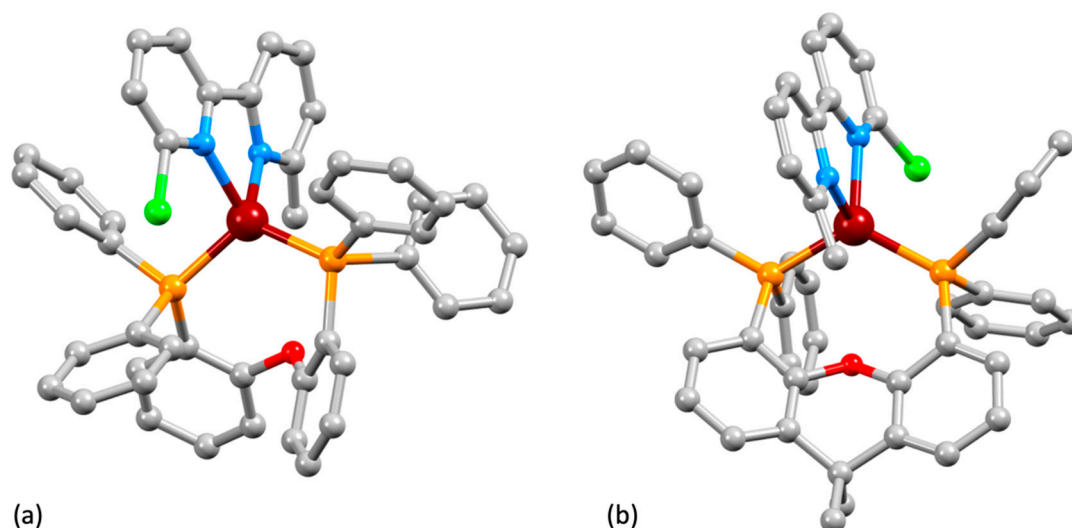
Figure 3. The structures of (**a**) the [Cu(POP)(6-Cl-6'-Mebpy)]$^+$ cation and (**b**) the [Cu(xantphos) (6-Cl-6'-Mebpy)]$^+$ cation in the hexafluoridophosphate salts; H atoms omitted. See Figures S12 and S14 for ORTEP representations and atom labeling. The figures show only one set of disordered sites in each complex (see text).

Table 1. Bond lengths and angles in the copper(I) coordination sphere in the cations in [Cu(POP)(6-Cl-6′-Mebpy)][PF$_6$] and [Cu(xantphos)(6-Cl-6′-Mebpy)][PF$_6$].

Cation	Cu–N/Å	Cu–P/Å	N–Cu–N/°	P–Cu–P/°	P–Cu–N/°
[Cu(POP)(6-Cl-6′-Mebpy)]$^+$	2.103(2), 2.131(3)	2.2497(11), 2.2774(13)	78.95(14)	116.51(5)	116.38(8), 112.11(8), 120.35(10), 106.79(11)
[Cu(xantphos)(6-Cl-6′-Mebpy)]$^+$	2.104(3), 2.123(3)	2.2750(13), 2.2978(13)	78.52(13)	120.36(5)	117.08(11), 105.66(10), 114.44(10), 113.21(11)

In [Cu(xantphos)(N^N)]$^+$ complexes which contain asymmetrical 6-substituted 2,2′-bipyridines or 2-(pyridin-2-yl)quinolines, the N^N ligand may favor a conformation in which the 6-substituent or quinoline unit lies over, or is remote from, the xanthene unit [11,12,18,19]. In some cases, NMR spectroscopy has provided evidence for mixtures of conformers in solution [11,18]. Among the 152 hits arising from a search of the Cambridge Structural Database (CSD, v. 5.4.1 [20]) for compounds containing a {Cu(POP/xantphos)(bpy/phen)} or closely related unit, only a few contain asymmetrical N^N ligands [10–12,14,18,21–23]. Within the context of these N^N ligands, 6-Cl-6′-Mebpy is atypical in being asymmetrical by virtue of having different substituents in the 6- and 6′-positions of the bpy domain. The disorder in [Cu(xantphos)(6-Cl-6′-Mebpy)][PF$_6$], modeled with equal occupancies of Cl and Me groups, indicates that there is no preference for the orientation of the 6-Cl-6′-Mebpy (Figure 4). This is consistent with the more general observation of similar steric effects for these two substituents [24,25].
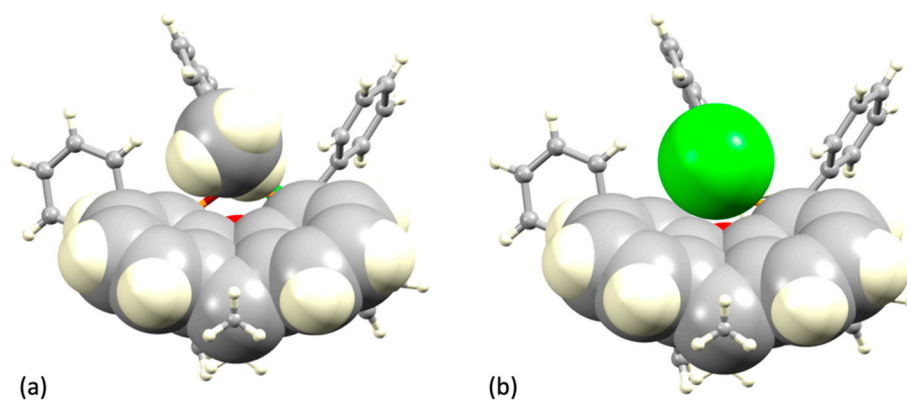
Figure 4. Hosting of the (**a**) methyl or (**b**) chloro substituent in the xanthene 'bowl' in [Cu(xantphos)(6-Cl-6′-Mebpy)][PF$_6$]. The structures are drawn using the two equal occupancy coordinates of the 6-Cl-6′-Mebpy ligand.

2.3. Electrochemical and Photophysical Properties of [Cu(POP)(6-Cl-6′-Mebpy)][PF$_6$] and [Cu(xantphos)(6-Cl-6′-Mebpy)][PF$_6$]

The electrochemical behavior of the copper(I) compounds was investigated using cyclic voltammetry. For the xantphos-containing compound, a reversible oxidation process (Figure 5 and Figure S15) was assigned to the Cu$^+$/Cu^{2+} redox process, but for [Cu(POP)(6-Cl-6′-Mebpy)][PF$_6$], the corresponding process was irreversible (Figure S16). Two ligand-centered reductive processes are observed for [Cu(POP)(6-Cl-6′-Mebpy)][PF$_6$] with values of E_{pa} = −2.03 and −2.21 V (Figure S16), but for the xantphos-containing complex, no reductive processes are observed within the solvent accessible window (Figure S15).
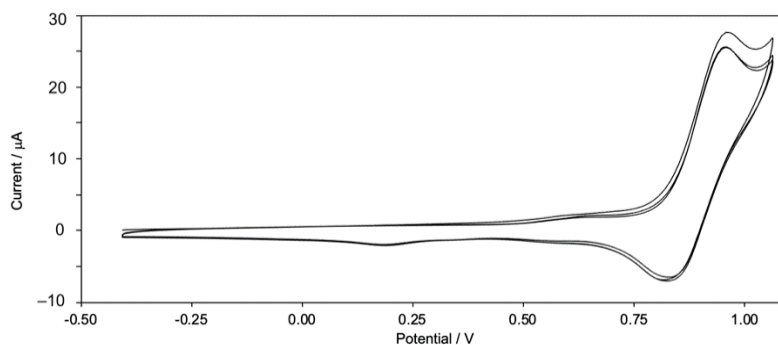
Figure 5. Three consecutive scans in the oxidative part of the cyclic voltammogram of [Cu(xantphos)(6-Cl-6′-Mebpy)][PF$_6$] in CH$_2$Cl$_2$ solution (ca. 10^{-4} mol dm^{-3}). [^{n}Bu$_4$N][PF$_6$] was used as the supporting electrolyte (scan rate = 0.1 V s^{-1}, reference Fc/Fc$^+$ = 0.0 V).

Table 2 compares values of the Cu$^+$/Cu^{2+} oxidation potential of [Cu(POP)(6-Cl-6′-Mebpy)]$^+$ and [Cu(xantphos)(6-Cl-6′-Mebpy)]$^+$ with those of the analogous complexes containing bpy, 6,6′-Me$_2$bpy and 6,6′-Cl$_2$bpy. Oxidation from copper(I) to copper(II) is accompanied by a change from preferred tetrahedral to square-planar geometry. On going from bpy to 6,6′-Me$_2$bpy, the shift in $E_{1/2}$ to higher potentials can be rationalized in terms of steric effects of the methyl substituents which hinder the flattening of the coordination sphere. In this case, steric effects appear to dominate over electronic effects since the electron-donating methyl substituents would also stabilize copper(II). On going from bpy or 6,6′-Me$_2$bpy to 6,6′-Cl$_2$bpy, the shift in $E_{1/2}$ to higher potentials is consistent with a combination of both steric and electronic effects; the electron-withdrawing chlorine substituents stabilize the copper(I) oxidation state. The value of $E_{1/2}$ for [Cu(xantphos)(6-Cl-6′-Mebpy)][PF$_6$] is in accord with an interplay of the effects of both chlorine and methyl groups, and the value of E_{pc} for [Cu(POP)(6-Cl-6′-Mebpy)][PF$_6$] is also consistent with this trend.

Table 2. Copper(I)/(II) oxidation potentials in [Cu(POP)(6-Cl-6′-Mebpy)][PF$_6$] and [Cu(xantphos)(6-Cl-6′-Mebpy)][PF$_6$] compared to those of related compounds. CH$_2$Cl$_2$ solutions (ca. 10^{-4} mol dm^{-3}); values are referenced to internal Fc/Fc$^+$ = 0.0 V; [^{n}Bu$_4$N][PF$_6$] as supporting electrolyte and scan rate of 0.1 V s^{-1}.

Compound	$E_{1/2}$ /V	$E_{pc} - E_{pa}$/mV	E_{pc} [a]/V	Reference
[Cu(POP)(6-Cl-6′-Mebpy)][PF$_6$]			+0.98	This work
[Cu(xantphos)(6-Cl-6′-Mebpy)][PF$_6$]	+0.91	106		This work
[Cu(POP)(6,6′-Cl$_2$bpy)][PF$_6$]	+0.98	170		[14]
[Cu(xantphos)(6,6′-Cl$_2$bpy)][PF$_6$]	+0.93	90		[14]
[Cu(POP)(6,6′-Me$_2$bpy)][BF$_4$]	+0.82 [b]	– [c]		[26]
[Cu(xantphos)(6,6′-Me$_2$bpy)][PF$_6$]	+0.90	150		[21]
[Cu(POP)(bpy)][PF$_6$]	+0.72	110		[21]
[Cu(xantphos)(bpy)][PF$_6$]	+0.76	110		[21]

[a] The value is given for E_{pc} when the process is irreversible. [b] In our hands, the compound shows only partial reversibility with E_{pc} = +0.93 V [27]. [c] No $E_{pc} - E_{pa}$ value reported.

Dichloromethane solutions of [Cu(POP)(6-Cl-6′-Mebpy)][PF$_6$] and [Cu(xantphos)(6-Cl-6′-Mebpy)][PF$_6$] exhibit absorption spectra comprising intense high-energy, ligand-centered absorptions and a broad, lower intensity band arising from metal-to-ligand charge transfer (MLCT). The spectra are shown in Figure 6a and data are presented in Table 3. The trend in the MLCT maximum on changing the NˆN ligand from bpy, 6,6′-Me$_2$bpy or 6,6′-Cl$_2$bpy to 6-Cl-6′-Mebpy reflects the changing electronic properties of the substituents. Figure 3b compares the MLCT absorptions of [Cu(xantphos)(6-Cl-6′-Mebpy)][PF$_6$], [Cu(xantphos)(bpy)][PF$_6$] [21], [Cu(xantphos)(6,6′-Me$_2$bpy)][PF$_6$] [11] and [Cu(xantphos)(6,6′-Cl$_2$bpy)][PF$_6$] [14]. The values of λ_{max} for the MLCT absorption are 400, 383, 379 and 420 nm, respectively. The LUMO of a [Cu(PˆP)(NˆN)]$^+$ complex is localized on the NˆN ligand, and introducing

electron-withdrawing chloro groups into the bpy unit stabilizes the LUMO with respect to that in [Cu(xantphos)(bpy)][PF$_6$] [14] or [Cu(xantphos)(6,6′-Me$_2$bpy)][PF$_6$], leading to a red shift in the MLCT absorption. A smaller red shift is observed when 6,6′-Cl$_2$bpy is replaced by 6-Cl-6′-Mebpy (Table 3 and Figure 3b), consistent with the combined characters of the N^N ligand.
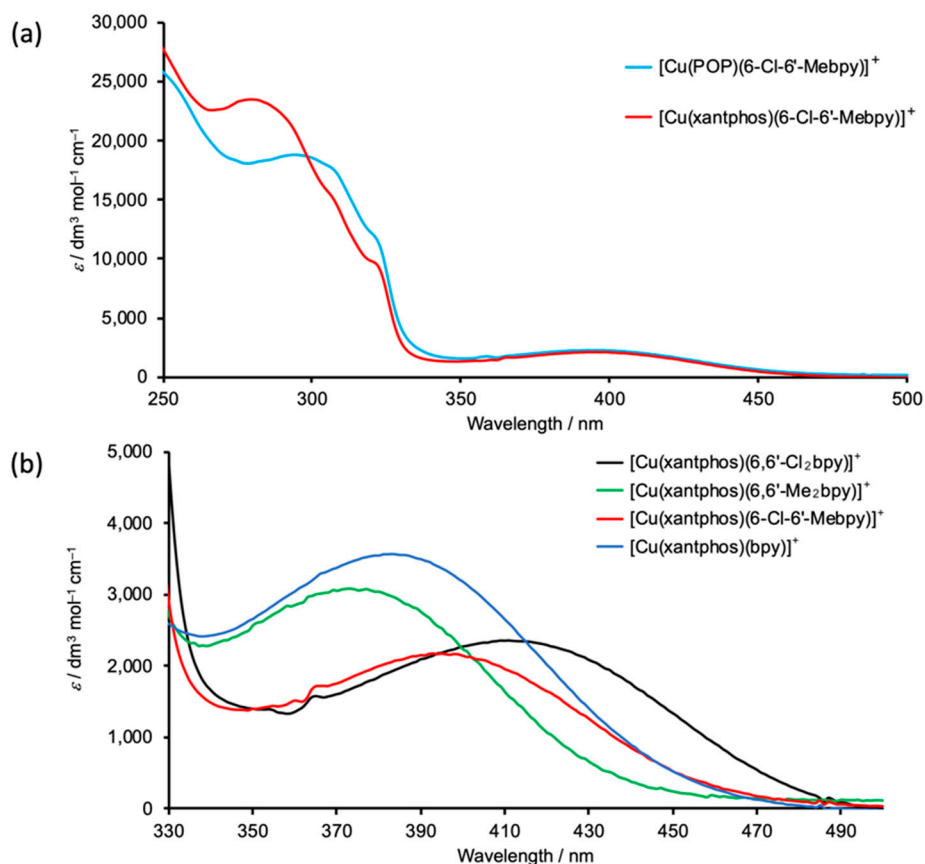

Figure 6. (**a**) The solution absorption spectra of [Cu(POP)(6-Cl-6′-Mebpy)][PF$_6$] and [Cu(xantphos)(6-Cl-6′-Mebpy)][PF$_6$] (CH$_2$Cl$_2$, 2.5×10^{-5} mol dm^{-3}). (**b**) Comparison of the metal-to-ligand charge transfer (MLCT) bands in the solution absorption spectra of [Cu(xantphos)(N^N)][PF$_6$] with N^N = bpy [21], 6,6′-Cl$_2$bpy [14], 6,6′-Me$_2$bpy [11] and 6-Cl-6′-Mebpy.

Table 3. Absorption maxima for CH$_2$Cl$_2$ solutions of [Cu(POP)(6-Cl-6′-Mebpy)][PF$_6$] and [Cu(xantphos)(6-Cl-6′-Mebpy)][PF$_6$] (2.5×10^{-5} mol dm^{-3}).

Compound	λ_{max}/nm (ε_{max}/dm^3 mol^{-1} cm^{-1})	
	$\pi^* \leftarrow \pi$	MLCT
[Cu(POP)(6-Cl-6′-Mebpy)][PF$_6$]	294 (18,800), 322 sh (11,500)	400 (2,160)
[Cu(xantphos)(6-Cl-6′-Mebpy)][PF$_6$]	283 (23,370), 307 sh (15,200), 322 sh (9,500)	400 (2,160)

When excited into the MLCT band at 400 nm, [Cu(POP)(6-Cl-6′-Mebpy)][PF$_6$] and [Cu(xantphos)(6-Cl-6′-Mebpy)][PF$_6$] are orange or yellow emitters (Table 4), and the solution and solid-state emission spectra are illustrated in Figure 7. In solution, the emission maximum of [Cu(POP)(6-Cl-6′-Mebpy)][PF$_6$] is at a longer wavelength compared to [Cu(xantphos)(Cl-Mebpy)][PF$_6$] with a redshift of 11 nm. The emission maxima of powdered samples are blue-shifted with respect to solution values (Table 4 and Figure 7) and again, the POP-containing complex is red shifted (by 10 nm) with respect to that containing the xantphos ligand. The solution emission bands exhibit a low-energy shoulder, consistent with the somewhat structured emissions observed for related [Cu(POP)(N^N)][PF$_6$] and [Cu(xantphos)(N^N)][PF$_6$] compounds [10,11,14]. As expected, the PLQY values are significantly

enhanced from solution to powdered samples (Table 4). The solid-state PLQY of 24% for [Cu(POP)(6-Cl-6'-Mebpy)][PF$_6$] lies between the 43.2% reported for [Cu(POP)(6,6'-Me$_2$bpy)][PF$_6$] [10] and the 14.8% observed for [Cu(POP)(6,6'-Cl$_2$bpy)][PF$_6$] [14]. The excited-state lifetime, τ, (which was determined using a biexponential fit [27] as detailed in Table 4) of 4.8 µs also lies between the values for [Cu(POP)(6,6'-Me$_2$bpy)][PF$_6$] (10.5 µs [10]) and [Cu(POP)(6,6'-Cl$_2$bpy)][PF$_6$] (2.7 µs [14]). Similar trends were seen for the xantphos-containing compounds with values of τ being 3.3, 4.0, and 11 µs for N^N = 6,6'-Cl$_2$bpy [14], 6-Cl-6'-Mebpy (Table 4) and 6,6'-Me$_2$bpy [10]. In terms of quantum yields, we observed that the PLQY of 16% for powdered [Cu(xantphos)(6-Cl-6'-Mebpy)][PF$_6$] compares with 37% reported for [Cu(xantphos)(6,6'-Me$_2$bpy)][PF$_6$] [11] and 17.1% observed for [Cu(xantphos)(6,6'-Cl$_2$bpy)][PF$_6$] [14].

Table 4. Photophysical properties of [Cu(POP)(6-Cl-6'-Mebpy)][PF$_6$] and [Cu(xantphos)(6-Cl-6'-Mebpy)][PF$_6$] and related compounds.

Compound	Solution (CH$_2$Cl$_2$, De-Aerated, 1.0×10^{-5} mol dm^{-3})				Powder					
	λ_{exc}/ nm	$\lambda_{max}{}^{em}$/ nm	PLQY/ %	τ/ns	λ_{exc}/ nm	$\lambda_{max}{}^{em}$/ nm	PLQY/ %	τ/µs^a	τ(1)/ µs (A$_1$)	τ(2)/ µs (A$_2$)
[Cu(POP)(6-Cl-6'-Mebpy)][PF$_6$]	400	593	5.5	1300	400	558	24	4.8	6.0 (0.66)	1.8 (0.25)
[Cu(xantphos)(6-Cl-6'-Mebpy)][PF$_6$]	400	582	1.4	420	400	548	16	4.0	6.0 (0.49)	1.3 (0.37)

^{a} A biexponential fit to the lifetime delay was used because a single exponential gave a poor fit; τ is calculated from the equation $\sum A_i \tau_i / \sum A_i$ and A_i is the pre-exponential factor for the lifetime and values of τ(1), τ(2), A$_1$ and A$_2$ are also given.
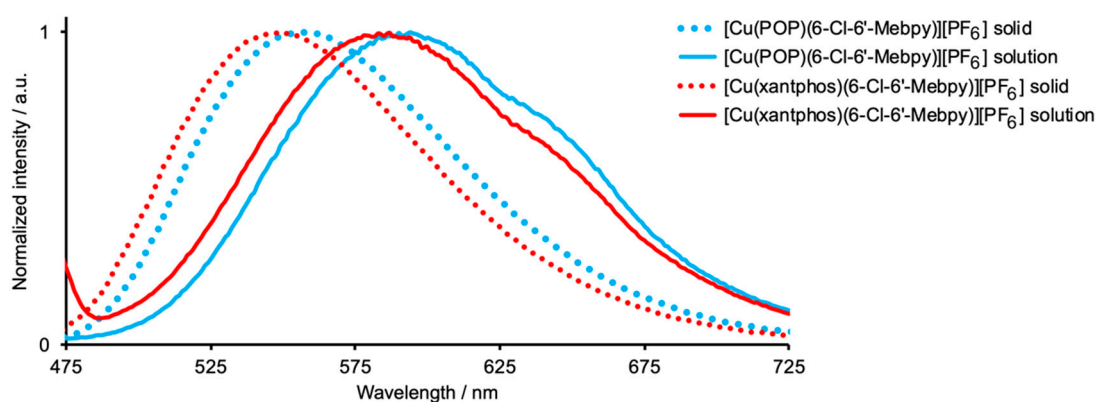

Figure 7. Emission spectra of powdered and solution (CH$_2$Cl$_2$, 1.0×10^{-5} mol dm^{-3}) samples of [Cu(POP)(6-Cl-6'-Mebpy)][PF$_6$] and [Cu(xantphos)(6-Cl-6'-Mebpy)][PF$_6$].

3. Materials and Methods

3.1. General

^{1}H, ^{13}C{^{1}H} and ^{31}P{^{1}H} NMR spectra were recorded at 298 K on a Bruker Avance III-500 NMR spectrometer (Bruker BioSpin AG, Fällanden, Switzerland). ^{1}H and ^{13}C NMR chemical shifts were referenced to residual solvent peaks with respect to δ(TMS) = 0 ppm and ^{31}P NMR chemical shifts with respect to δ(85% aqueous H$_3$PO$_4$) = 0 ppm. Shimadzu LCMS-2020 (Shimadzu Schweiz GmbH, Reinach, Switzerland) and Bruker esquire 3000plus instruments (Bruker BioSpin AG, Fällanden, Switzerland) were used to record electrospray ionization (ESI) mass spectra with samples introduced. Solution absorption and emission spectra were recorded using an Agilent 8453 spectrophotometer (Agilent Technologies, Inc., Santa Clara, CA, USA) and Shimadzu RF-5301PC spectrofluorometer (Shimadzu Schweiz GmbH, Reinach, Switzerland), respectively. A Hamamatsu absolute photoluminescence

quantum yield spectrometer C11347 Quantaurus-QY (Hamamatsu Photonics France, Solothurn, Switzerland) was used to measure PLQYs and emission lifetimes and powder emission spectra were measured using a Hamamatsu Compact Fluorescence lifetime Spectrometer C11367 Quantaurus-Tau with an LED light source (λ_{exc} = 365 nm). Microwave reactions were performed in a Biotage Initiator 8 microwave reactor (Biotage EU, 75103 Uppsala, Sweden).

Cyclic voltammograms were recorded using a CH Instruments 900B potentiostat (CH Instruments, Bee Cave, TX, USA) with [$^nBu_4N$][PF_6] (0.1 mol dm^{-3}) as the supporting electrolyte and a scan rate of 0.1 V s^{-1}; the solvent was HPLC grade CH_2Cl_2 and solution concentrations were ca. 1×10^{-4} mol dm^{-3}. All solutions were degassed with argon. The working electrode was glassy carbon, the reference electrode was an Ag wire, and the counter-electrode was a Pt wire. Final potentials were internally referenced with respect to the Fc/Fc$^+$ couple.

POP and xantphos were bought from Acros (Fisher Scientific AG, Reinach, Switzerland) and Fluorochem (Chemie Brunschwig AG, Basel, Switzerland), respectively. (6-Methylpyridin-2-yl)zinc(II) bromide was purchased from Sigma-Aldrich (Sigma Aldrich Chemie GmbH, Steinheim, Germany). [$Cu(MeCN)_4$][PF_6] was prepared as described in the literature [28].

3.2. 6-Chloro-6′-methyl-2,2′-bipyridine (6-Cl-6′-Mebpy)

A microwave vial (20 mL) was evacuated and backfilled three times with N_2. Then [$Pd(PPh_3)_4$] (393 mg, 3.40×10^{-4} mmol, 4.6 mol %), 2,6-dichloropyridine (1.00 g, 6.76 mmol, 1.0 eq.) and 6-methyl-2-pyridinylzinc bromide (0.5 M in THF, 13.5 mL, 13.5 g, 6.76 mmol, 1.0 eq.) were added to the vial. The solution was degassed with N_2 for 20 min. The reaction was carried out in a microwave reactor for 2 h at 110 °C, during which time, a precipitate formed. Aqueous saturated $NaHCO_3$ (15 mL) and brine (15 mL) were added to the reaction mixture and this was then diluted with Milli-Q water to improve the separation of the organic and aqueous layers. The mixture was extracted with CH_2Cl_2 (3 × 20 mL). The combined organic layers were washed with H_2O (3 × 20 mL), dried over $MgSO_4$ and the solvent was removed under reduced pressure. After purification by column chromatography (silica; cyclohexane/EtOAc 20:1; Rf = 0.24), 6-Cl-6′-Mebpy was isolated as a colorless oil (0.326 g, 1.59 mmol, 23.5%). ^1H NMR (500 MHz, 298 K, CDCl$_3$) δ/ppm: 8.38 (d, J = 7.6 Hz, 1H, H^{B3}), 8.20 (d, J = 7.8 Hz, 1H, H^{A3}), 7.76 (m, 1H, H^{B4}), 7.70 (m, 1H, H^{A4}), 7.32 (m, 1H, H^{B5}), 7.19 (d, J = 7.6 Hz, 1H, H^{A5}), 2.63 (s, 3H, H^{Me}). $^{13}C\{^1H\}$ NMR (126 MHz, 298 K, CDCl$_3$) δ/ppm 158.2 (C^{A6}), 157.3 (C^{B2}), 154.1 (C^{A2}), 150.9 (C^{B6}), 139.5 (C^{B4}), 137.4 (C^{A4}), 124.1 (C^{B5}), 124.0 (C^{A5}), 119.5 (C^{B3}), 118.6 (C^{A3}), 24.5 (C^{Me}). ESI-MS (CH$_2$Cl$_2$/MeOH, positive mode) *m/z* 205.02 [M + H]$^+$ (base peak, calc. 205.05).

3.3. [Cu(POP)(6-Cl-6′-Mebpy)][PF$_6$]

[$Cu(MeCN)_4$][PF_6] (93.3 mg, 0.250 mmol, 1.0 eq.) and POP (162 mg, 0.300 mmol, 1.2 eq.) were dissolved in CH_2Cl_2 (30 mL) and the mixture was stirred for 2 h at room temperature. Then 6-Cl-6′-Mebpy (51.3 mg, 0.250 mmol, 1.0 eq.) was added to the mixture and this was stirred for 2 h. The mixture was filtered and the solvent from the filtrate was removed under vacuum to give a yellow solid. The product was purified by precipitation with Et$_2$O (4 times) from a CH_2Cl_2 solution of the compound and was finally isolated after sonication (5 min) and centrifugation (3000 rpm, 3 min). [Cu(POP)(6-Cl-6′-Mebpy)][PF$_6$] was obtained as a yellow crystalline solid (172 mg, 0.180 mmol, 72.0%). ^1H NMR (500 MHz, 298 K, acetone-d_6) δ/ppm 8.40 (d, J = 7.9 Hz, 1H, H^{B3}), 8.33 (d, J = 8.0 Hz, 1H, H^{A3}), 8.16 (m, 1H, H^{B4}), 8.09 (m, 1H, H^{A4}), 7.68 (d, J = 7.9 Hz, 1H, H^{B5}), 7.43 (d, J = 7.8 Hz, 1H, H^{A5}), 7.41–7.35 (overlapping m, 8H, H$^{C5+D2+D4}$), 7.33 (m, 2H, H$^{D4'}$), 7.23–7.29 (overlapping m, 6H, H^{C4+D3}), 7.22–7.15 (overlapping m, 6H, H$^{C3+D3'}$), 7.04–6.97 (overlapping m, 6H, H$^{C6+D2'}$), 2.07 (s, 3H, H^{Me}). $^{13}C\{^1H\}$ NMR (126 MHz, acetone-d_6) δ/ppm 160.6 (C^{A6}), 158.8 (t, J_{CP} = 6 Hz, C^{C1}), 154.9 (C^{B2}), 152.1 (C^{A2}), 151.7 (C^{B6}), 142.6 (C^{B4}), 140.1 (C^{A4}), 135.2 (t, J_{CP} = 8 Hz, C^{D2}), 134.4 (C^{C3}), 133.2 (C^{C5}), 133.0 (t, J_{CP} = 6 Hz, C$^{D2'}$), 132.6 (t, J_{CP} = 17 Hz, C$^{D1+D1'}$), 131.2 (C^{D4}), 130.5 (C$^{D4'}$), 129.6 (t, J_{CP} = 4 Hz, C$^{D3+D3'}$), 128.1 (C^{A5}), 127.4 (C^{B5}), 126.4 (t, J_{CP} = 15 Hz, C^{C2}), 126.1 (t, J_{CP} = 2 Hz, C^{C4}), 122.4 (C^{B3}), 121.5 (C^{A3}), 120.8 (t, J_{CP} = 2 Hz, C^{C6}), 25.9 (C^{Me}). $^{31}P\{^1H\}$ NMR (202 MHz, 298 K, acetone-d_6) δ/ppm

−13.0 (broad, POP), −144.3 (heptet, J_{PF} = 707 Hz, $PF_6{}^-$). ESI-MS (CH_2Cl_2/MeOH, positive mode) m/z 805.12 $[M − PF_6]^+$ (calc. 805.14), 601.09 $[M − PF_6 − (6\text{-Cl-}6'\text{-Mebpy})]^+$ (base peak, calc. 601.09). Found: C 58.56, H 4.04, N 2.85; $C_{47}H_{37}ClCuF_6N_2OP_3$ requires C 59.31, H 3.92, N 2.94.

3.4. [Cu(xantphos)(6-Cl-6′-Mebpy)][PF₆]

[Cu(MeCN)₄][PF₆] (94.5 mg, 0.253 mmol, 1.0 eq.), xantphos (146.7 mg, 0.253 mmol, 1.0 eq.) and 6-Cl-6′-Mebpy (52.1 mg, 0.250 mmol, 1.0 eq.) were dissolved in CH_2Cl_2 (30 mL) and the mixture was stirred for 4 h at room temperature. The mixture was filtered and the solvent from the filtrate was removed in vacuo yielding a yellow solid. The product was purified by precipitation with Et_2O (4 times) from a CH_2Cl_2 solution and was finally isolated after sonication (5 min) and centrifugation (3000 rpm, 3 min). [Cu(xantphos)(6-Cl-6′-Mebpy)][PF₆] was obtained as a yellow crystalline solid (219 mg, 0.220 mmol, 87.0%). ^{1}H NMR (500 MHz, 298 K, acetone-d_6) δ/ppm 8.31 (d, J = 7.8 Hz, 1H, H^{B3}), 8.23 (d, J = 7.9 Hz, 1H, H^{A3}), 8.12 (m, 1H, H^{B4}), 8.04 (m, 1H, H^{A4}), 7.82 (dd, J = 7.8, 1.4 Hz, 2H, C^{C5}), 7.60 (d, J = 7.6 Hz, 1H, H^{B5}), 7.46 (d, J = 7.8 Hz, 1H, H^{A5}), 7.41 (m, 4H, $H^{D4+D4'}$), 7.30 (m, 2H, H^{C4}), 7.28–7.20 (overlapping m, 12H, $H^{D2+D3+D3'}$), 7.13 (m, 4H, $H^{D2'}$), 6.97 (m, 2H, H^{C3}), 2.06 (s, 3H, $H^{bpy\text{-Me}}$), 1.79 (s, 3H, $H^{xantphos\text{-Me}}$), 1.69 (s, 3H, $H^{xantphos\text{-Me}}$). ^{13}C{^{1}H} NMR (126 MHz, 298 K, acetone-d_6) δ/ppm 159.6 (C^{A6}), 155.9 (t, J_{CP} = 6 Hz, C^{C1}), 154.2 (C^{B2}), 151.7 (C^{A2}), 142.5 (C^{B4}), 140.1 (C^{A4}), 134.6 (t, J_{CP} = 2 Hz, C^{C6}), 134.2 (t, J_{CP} = 8 Hz, C^{D2}), 134.0 (t, J_{CP} = 8 Hz, $C^{D2'}$), 132.4 (m, $C^{D1+D1'}$), 131.1 (C^{C3}), 131.0 ($C^{D4/D4'}$), 130.95 ($C^{D4/D4'}$), 129.8 (t, J_{CP} = 5 Hz, $C^{D3/D3'}$), 129.5 (t, J_{CP} = 5 Hz, $C^{D3/D3'}$), 128.6 (C^{C5}), 127.5 (C^{A5}), 127.2 (C^{B5}), 126.2 (t, J_{CP} = 2 Hz, C^{C4}), 122.6 (t, J_{CP} = 13 Hz, C^{C2}), 122.2 (C^{B3}), 121.5 (C^{A3}), 36.8 ($C^{xantphos\text{-bridge}}$), 29.5 ($C^{xantphos\text{-Me}}$), 28.1 ($C^{xantphos\text{-Me}}$), 26.8 ($C^{bpy\text{-Me}}$). ^{31}P{^{1}H} NMR (202 MHz, 298 K, acetone-d_6) δ/ppm −13.5 (broad, xantphos), −144.3 (heptet, J_{PF} = 707, $PF_6{}^-$). ESI-MS (CH_2Cl_2/MeOH, positive mode) m/z 845.16 $[M − PF_6]^+$ (calc. 845.17), 641.10 $[M − PF_6 − (6\text{-Cl-}6'\text{-Mebpy})]^+$ (base peak, calc. 641.12). Found: C 58.63, H 4.11, N 2.71; $C_{50}H_{41}ClCuF_6N_2OP_3 \cdot 0.5CH_2Cl_2$ requires C 58.65, H 4.09, N 2.71.

3.5. Crystallography

Single crystal data were collected on a STOE StadiVari diffractometer (STOE & Cie GmbH, Darmstadt, Germany) equipped with a Pilatus300K detector and a Metaljet D2 source (Ga Kα radiation). The structure was solved using Superflip [29,30] and CRYSTALS [31]. Structure analysis including the ORTEP representations, used Mercury CSD v. 4.1.1 [32,33]. The cation in [Cu(POP)(6-Cl-6′-Mebpy)][PF₆] suffered from severe disorder and all the aromatic rings were refined as rigid bodies; one ring was refined isotropically as it was not possible to identify two distinct orientations, and the C atom of the methyl group was also refined isotropically. In the 6-Cl-6′-Mebpy ligand in [Cu(xantphos)(6-Cl-6′-Mebpy)][PF₆], the Cl/Me sites were disordered and were modeled over two sites with equal occupancies.

3.6. [Cu(POP)(6-Cl-6′-Mebpy)][PF₆]

$C_{47}H_{37}ClCuF_6N_2OP_3$, M_r = 951.73, yellow block, monoclinic, space group $P2_1/c$, a = 10.4786(3), b = 18.9864(4), c = 22.1096(5) Å, β = 100.077(2)°, V = 4330.87(18) Å^3, D_c = 1.460 g cm^{-3}, T = 130 K, Z = 4, μ(GaKα) = 4.150 mm^{-1}. Total 48,628 reflections, 8755 unique (R_{int} = 0.035). Refinement of 7234 reflections (539 parameters) with $I > 2\sigma(I)$ converged at final R_1 = 0.1124 (R_1 all data = 0.1124), wR_2 = 0.0443 (wR_2 all data = 0.0443), gof = 1.0315. CCDC 1995549.

3.7. [Cu(xantphos)(6-Cl-6′-Mebpy)][PF₆]

$C_{50}H_{41}ClCuF_6N_2OP_3$, M_r = 991.80, yellow plate, triclinic, space group $P−1$, a = 11.4363(6), b = 14.0871(6), c = 14.8030(7) Å, α = 89.133(4), β = 68.457(4), γ = 88.730(4)°, V = 2217.62(19) Å^3, D_c = 1.485 g cm^{-3}, T = 130 K, Z = 2, μ(Ga Kα) = 4.068 mm^{-1}. Total 23,726 reflections, 8675 unique (R_{int} = 0.045). Refinement of 7234 reflections (539 parameters) with $I > 2\sigma(I)$ converged at final R_1 = 0.1112 (R_1 all data = 0.1112), wR_2 = 0.0483 (wR_2 all data = 0.0483), gof = 0.9937. CCDC 1995548.

4. Conclusions

We have described the synthesis and characterization of the asymmetrical ligand 6-Cl-6'-Mebpy. This was incorporated into the copper(I) compounds [Cu(POP)(6-Cl-6'-Mebpy)][PF$_6$] and [Cu(xantphos)(6-Cl-6'-Mebpy)] [PF$_6$], both of which were structurally characterized. The copper(I) ion is in a distorted tetrahedral environment and in [Cu(xantphos)(6-Cl-6'-Mebpy)][PF$_6$], the disorder of the 6-Cl-6'-Mebpy ligand indicates that there is no preference for the 'bowl'-like cavity of the xanthene unit to host either the methyl or chloro-substituent, consistent with similar steric effects of the two groups.

[Cu(xantphos)(6-Cl-6'-Mebpy)][PF$_6$] and [Cu(POP)(6-Cl-6'-Mebpy)][PF$_6$] undergo a reversible and irreversible copper(I) oxidation, respectively. A comparison with reported data [14,21,26] for [Cu(PˆP)(NˆN)]$^+$ complexes in which PˆP = POP and xantphos and NˆN = 6,6'-Cl$_2$bpy and 6,6'-Me$_2$bpy reveals that values for [Cu(PˆP)(6-Cl-6'-Mebpy)]$^+$ are consistent with there being an interplay of the effects of both chloro and methyl groups. The photophysical properties also support these combined effects. For example, the xantphos-containing compounds, values of λ_{max} for the MLCT absorption are 379, 400 and 420 nm, respectively, for NˆN = 6,6'-Me$_2$bpy, 6-Cl-6'-Mebpy and 6,6'-Cl$_2$bpy. For the POP-containing complexes, the solid-state emission maxima appear at 535, 558 and 584 nm, respectively, for NˆN = 6,6'-Me$_2$bpy, 6-Cl-6'-Mebpy and 6,6'-Cl$_2$bpy, with PLQY values of 43.2%, 24% and 14.8% and excited state lifetimes of 10.5, 4.8 and 2.7 μs, respectively.

Supplementary Materials: The following are available online at http://www.mdpi.com/2304-6740/8/5/33/s1, Figure S1: Electrospray mass spectrum of 6-Cl-6'-Mebpy; Figures S2–S4: NMR spectra of 6-Cl-6'-Mebpy; Figures S5–S6: Electrospray mass spectra of [Cu(POP)(6-Cl-6'-Mebpy)][PF$_6$] and [Cu(xantphos)(6-Cl-6'-Mebpy)][PF$_6$]; Figures S7–S11: NMR spectra of the complexes; Figures S12–S14: Additional structural figures; Figures S15–S16: Cyclic voltammograms. Cif and CheckCif files of [Cu(POP)(6-Cl-6'-Mebpy)][PF$_6$] and [Cu(xantphos)(6-Cl-6'-Mebpy)][PF$_6$].

Author Contributions: Project conceptualization, administration, supervision and funding acquisition, E.C.C. and C.E.H.; investigation, M.M. and F.B.; data analysis, M.M.; crystallography, A.P.; writing, C.E.H., M.M.; manuscript editing, M.M., F.B., E.C.C., A.P. All authors have read and agreed to the published version of the manuscript.

Conflicts of Interest: The authors declare no conflict of interest.

References

1. Lighting the Future. Available online: https://ec.europa.eu/digital-single-market/en/lighting-future (accessed on 27 March 2020).

2. Costa, R.D. (Ed.) *Light-Emitting Electrochemical Cells: Concepts, Advances and Challenges*; Springer International Publishing: New York, NY, USA, 2017. [CrossRef]

3. Fresta, E.; Costa, R.D. Beyond traditional light-emitting electrochemical cells—A review of new device designs and emitters. *J. Mater. Chem. C* **2017**, *5*, 5643–5675. [CrossRef]

4. Kamer, P.C.J.; van Leeuwen, P.W.N.M.; Reek, J.N.H. Wide Bite Angle Diphosphines: Xantphos Ligands in Transition Metal Complexes and Catalysis. *Acc. Chem. Rev.* **2001**, *34*, 895–904. [CrossRef] [PubMed]

5. Buckner, M.T.; McMillin, D.R. Photoluminescence from copper(I) complexes with low-lying metal-to-ligand charge transfer excited states. *J. Chem. Soc. Chem. Commun.* **1978**, 759–761. [CrossRef]

6. Rader, R.A.; McMillin, D.R.; Buckner, M.T.; Matthews, T.G.; Casadonte, D.J.; Lengel, R.K.; Whittaker, S.B.; Darmon, L.M.; Lytle, F.E. Photostudies of 2,2'-bipyridine bis(triphenylphosphine)copper(1+), 1,10-phenanthroline bis(triphenylphosphine)copper(1+), and 2,9-dimethyl-1,10-phenanthroline bis(triphenylphosphine)copper(1+) in solution and in rigid, low-temperature glasses. Simultaneous multiple emissions from intraligand and charge-transfer states. *J. Am. Chem. Soc.* **1981**, *103*, 5906–5912. [CrossRef]

7. Czerwieniec, R.; Leitl, M.J.; Homeier, H.H.H.; Yersin, H. Cu(I) complexes—Thermally activated delayed fluorescence. Photophysical approach and material design. *Coord. Chem. Rev.* **2016**, *325*, 2–28. [CrossRef]

8. Bergmann, L.; Zink, D.M.; Bauman, T.; Volz, D.; Bräse, S. Metal-Organic and Organic TADF Materials: Status, Challenges and Characterization. *Top. Curr. Chem.* **2016**, *374*, 22. [CrossRef]

9. Elie, M.; Gaillard, S.; Renaud, J.-L. *Light-Emitting Electrochemical Cells*; Costa, R.D., Ed.; Springer International Publishing: Cham, Swizerland, 2017; pp. 287–327. [CrossRef]

10. Keller, S.; Constable, E.C.; Housecroft, C.E.; Neuburger, M.; Prescimone, A.; Longo, G.; Pertegás, A.; Sessolo, M.; Bolink, H.J. [Cu(bpy)(PˆP)]$^+$ containing light-emitting electrochemical cells: Improving performance through simple substitution. *Dalton Trans.* **2014**, *43*, 16593–16596. [CrossRef]

11. Keller, S.; Pertegás, A.; Longo, G.; Martínez, L.; Cerdá, J.; Junquera-Hernández, J.M.; Prescimone, A.; Constable, E.C.; Housecroft, C.E.; Ortí, E.; et al. Shine bright or live long: Substituent effects in [Cu(NˆN)(PˆP)]$^+$-based light-emitting electrochemical cells where NˆN is a 6-substituted 2,2′-bipyridine. *J. Mater. Chem. C* **2016**, *4*, 3857–3871. [CrossRef]

12. Alkan-Zambada, M.; Keller, S.; Martínez-Sarti, L.; Prescimone, A.; Junquera-Hernández, J.M.; Constable, E.C.; Bolink, H.J.; Sessolo, M.; Ortí, E.; Housecroft, C.E. [Cu(PˆP)(NˆN)][PF$_6$] compounds with bis(phosphane) and 6-alkoxy, 6-alkylthio, 6-phenyloxy and 6-phenylthio-substituted 2,2′-bipyridine ligands for light-emitting electrochemical cells. *J. Mater. Chem. C* **2018**, *6*, 8460–8471. [CrossRef]

13. Fresta, E.; Volpi, G.; Milanesio, M.; Garino, C.; Barolo, C.; Costa, R.D. Novel Ligand and Device Designs for Stable Light-Emitting Electrochemical Cells Based on Heteroleptic Copper(I) Complexes. *Inorg. Chem.* **2018**, *57*, 10469–10479. [CrossRef]

14. Keller, S.; Prescimone, A.; Bolink, H.J.; Sessolo, S.; Longo, G.; Martínez-Sarti, L.; Junquera-Hernández, J.M.; Constable, E.C.; Ortí, E.; Housecroft, C.E. Luminescent copper(I) complexes with bisphosphane and halogen-substituted 2,2′-bipyridine ligands. *Dalton Trans.* **2018**, *47*, 14263–14276. [CrossRef] [PubMed]

15. Costa, R.D.; Tordera, D.; Ortí, E.; Bolink, H.J.; Schönle, J.; Graber, S.; Housecroft, C.E.; Constable, E.C.; Zampese, J.A. Copper(I) Complexes for Sustainable Light-Emitting Electrochemical Cells. *J. Mater. Chem.* **2011**, *21*, 16108–16118. [CrossRef]

16. Zambach, W.; Quaranta, L.; Massol-Frieh, C.; Trah, S.; Stierli, D.; Pouliot, M.; Nebel, K. Novel Microbiocides. Patent WO 2013026866A2, 28 February 2013.

17. Sánchez-Castellanos, M.; Flores-Leonar, M.M.; Mata-Pinzón, Z.; Laguna, H.G.; García-Ruiz, K.M.; Rozenel, S.S.; Ugalde-Saldívar, V.M.; Moreno-Esparza, R.; Pijpers, J.J.H.; Amador-Bedolla, C. Theoretical exploration of 2,2′-bipyridines as electro-active compounds in flow batteries. *Phys. Chem. Chem. Phys.* **2019**, *21*, 15823–15832. [CrossRef] [PubMed]

18. Brunner, F.; Graber, S.; Baumgartner, Y.; Häussinger, D.; Prescimone, A.; Constable, E.C.; Housecroft, C.E. The effects of introducing sterically demanding aryl substituents in [Cu(NˆN)(PˆP)]$^+$ complexes. *Dalton Trans.* **2017**, *46*, 6379–6391. [CrossRef] [PubMed]

19. Keller, S.; Alkan-Zambada, M.; Prescimone, A.; Constable, E.C.; Housecroft, C.E. Extended π-Systems in Diimine Ligands in [Cu(PˆP)(NˆN)][PF$_6$] Complexes: From 2,2′-Bipyridine to 2-(Pyridin-2-yl)quinoline. *Crystals* **2020**, *10*, 255. [CrossRef]

20. Groom, C.R.; Bruno, I.J.; Lightfoot, M.P.; Ward, S.C. The Cambridge Structural Database. *Acta Cryst.* **2016**, *B72*, 171–179. [CrossRef]

21. Keller, S.; Brunner, F.; Junquera-Hernández, J.M.; Pertegás, A.; La-Placa, M.-G.; Prescimone, A.; Constable, E.C.; Bolink, H.J.; Ortí, E.; Housecroft, C.E. CF$_3$ Substitution of [Cu(PˆP)(bpy)][PF$_6$] complexes: Effects on Photophysical Properties and Light-emitting Electrochemical Cell Performance. *ChemPlusChem* **2018**, *83*, 217–229. [CrossRef]

22. Brunner, F.; Babaei, A.; Pertegás, A.; Junquera-Hernández, J.M.; Prescimone, A.; Constable, E.C.; Bolink, H.J.; Sessolo, M.; Ortí, E.; Housecroft, C.E. Phosphane tuning in heteroleptic [Cu(NˆN)(PˆP)]$^+$ complexes for light-emitting electrochemical cells. *Dalton Trans.* **2019**, *48*, 446–460. [CrossRef]

23. Alkan-Zambada, M.; Hu, X. Cu Photoredox Catalysts Supported by a 4,6-Disubstituted 2,2′-Bipyridine Ligand: Application in Chlorotrifluoromethylation of Alkenes. *Organometallics* **2018**, *21*, 3928–3935. [CrossRef]

24. MacPhee, J.A.; Panaye, A.; Dubois, J.-E. Steric Effects—I: A Critical Examination of the Taft Steric Parameter – E$_S$. Definition of a revised, broader and homogeneous scale. Extension to highly congested alkyl groups. *Tetrahedron* **1978**, *34*, 3553–3562. [CrossRef]

25. Belot, V.; Farran, D.; Jean, M.; Albalat, M.; Vanthuyne, N.; Roussel, C. Steric Scale of Common Substituents from Rotational Barriers of *N*-(*o*-Substituted aryl)thiazoline-2-thione Atropisomers. *J. Org. Chem.* **2017**, *82*, 10188–10200. [CrossRef] [PubMed]

26. Andrés-Tomé, I.; Fyson, J.; Baiao Dias, F.; Monkman, A.P.; Iacobellis, G.; Coppo, P. Copper(I) complexes with bipyridyl and phosphine ligands: A systematic study. *Dalton Trans.* **2012**, *41*, 8669–8674. [CrossRef] [PubMed]

27. Hofbeck, T.; Monkowius, U.; Yersin, H. Highly Efficient Luminescence of Cu(I) Compounds: Thermally Activated Delayed Fluorescence Combined with Short-Lived Phosphorescence. *J. Am. Chem. Soc.* **2015**, *137*, 399–404. [CrossRef]

28. Kubas, G.J.; Monzyk, B.; Crumbliss, A.L. Tetrakis(acetonitrile)copper(I) hexafluorophosphate. *Inorg. Synth.* **1979**, *19*, 90–92. [CrossRef]

29. Palatinus, L.; Chapuis, G. Superflip—A Computer Program for the Solution of Crystal Structures by Charge Flipping in Arbitrary Dimensions. *J. Appl. Cryst.* **2007**, *40*, 786–790. [CrossRef]

30. Palatinus, L.; Prathapa, S.J.; van Smaalen, S. EDMA: A Computer Program for Topological Analysis of Discrete Electron Densities. *J. Appl. Cryst.* **2012**, *45*, 575–580. [CrossRef]

31. Betteridge, P.W.; Carruthers, J.R.; Cooper, R.I.; Prout, K.; Watkin, D.J. CRYSTALS version 12: Software for guided crystal structure analysis. *J. Appl. Cryst.* **2003**, *36*, 1487. [CrossRef]

32. Macrae, C.F.; Edgington, P.R.; McCabe, P.; Pidcock, E.; Shields, G.P.; Taylor, R.; Towler, M.; van de Streek, J. Mercury: Visualization and Analysis of Crystal Structures. *J. Appl. Cryst.* **2006**, *39*, 453–457. [CrossRef]

33. Macrae, C.F.; Bruno, I.J.; Chisholm, J.A.; Edgington, P.R.; McCabe, P.; Pidcock, E.; Rodriguez-Monge, L.; Taylor, R.; van de Streek, J.; Wood, P.A. Mercury CSD 2.0—New Features for the Visualization and Investigation of Crystal Structures. *J. Appl. Cryst.* **2008**, *41*, 466–470. [CrossRef]